Desalination and Water Treatment
www.deswater.com

doi: 10.5004/dwt.2018.22310

115 (2018) 271–280
May

Removal of methyl orange from aqueous solutions by polydopamine-mediated surface functionalization of Fe_3O_4 in batch mode

Minyuan Han, Qing Wang, Hui Li, Liyan Fang, Runping Han*

College of Chemistry and Molecular Engineering, Zhengzhou University, No 100 of Kexue Road, Zhengzhou, 450001, China, email: 2455459591@qq.com (M. Han), 565734174@qq.com (Q. Wang), 15737156012@qq.com (H. Li), 867839030@qq.com (L. Fang), Tel. +86 371 67781757, Fax +86 371 67781556, email: rphan67@zzu.edu.cn (R. Han)

Received 31 January 2018; Accepted 2 April 2018

ABSTRACT

The magnetic core-shell polyethylenimine/polydopamine/Fe_3O_4 (PEI@PDA@Fe_3O_4) composites were facilely prepared by PEI functionalized Fe_3O_4 utilizing PDA as a mediator and were used to remove methyl orange (MO) from aqueous solution. The morphology and structure of the Fe_3O_4 and PEI@PDA@Fe_3O_4 were confirmed using automatic element analyzer (EA), X-Ray diffractometer (XRD), scanning electron microscopy (SEM) and point zero charge (pH_{pzc}). Several factors, such as contact time, adsorbent dosage, initial solution pH values, co-existing anions, initial MO concentration and solution temperature, were selected to study the effect on adsorption quantity. The solution pH was favored of MO adsorption at pH 3 while the coexist ion of common salt in solution was opposite. In addition, the kinetic data were described better by the Elovich equation and Double Constant model. The adsorption isotherm had a good fit with Langmuir model and Koble Corrigan model. The maximum MO adsorption capacity was 133 mg/g at 313 K. Thermodynamic parameters indicated that the MO adsorption process was endothermic and spontaneous in nature. Spent adsorbent can be regenerated using 0.010 mol/L HCl solution.

Keywords: Polyethylenimine/polydopamine/Fe_3O_4 composites; Methyl orange; Adsorption

1. Introduction

Dyeing effluent is widely discharged in the textile industry, paper printing, pharmaceutical, food, cosmetics, and other industries. These synthetic dyes, especially azo dyes, can cause toxic and mutagenic [1]. So removal of these dyes is important and necessary. There were many physicochemical methods for the removal of dyes from wastewater, including adsorption [2], biological treatment technology [3], membrane filtration [4], coagulation/flocculation [5], etc. Most of these conventional methods were either ineffective or high operational costs except for adsorption method [2]. The traditional adsorbents such as activate carbon [6], peanut husk [7], wheat straw [8], alginate beads [9] had mainly adopted the centrifugation or filter, which has the problem of separation difficulty in practical application, and also easily causes the clogging of the screen or the loss of the activated carbon [10].

In recent years, magnetic adsorbents have attracted attention because they could be easily separated from water in short time, spend low operational costs and not produce any pollutants, over other separation methods [11]. Fe_3O_4 was often used because of its magnetism and large surface area [12]. Direct use of magnetic materials for removal of dyes was relatively low efficiency. So modified magnetic materials such as MCH-La [13] and Fe-Si-La [11] were reported for removal of fluoride and phosphate from solution. Polyethylenimine (PEI) has a high amine density that has electrostatic effect, ion exchange and chelating ligands combined with a variety of pollutants. However, the good water solubility of PEI molecules limits it direct adsorption on fields of water treatment [14]. Polydopamine (PDA) can be produced from dopamine, which can spontaneously deposit a thin film on any material surface.

*Corresponding author.

PDA coatings have been found to be an extremely versatile secondary reaction platform that provides different coatings for a variety of uses [15]. In addition, some researchers have taken advantage of PDA deposition followed by PEI grafting on polyethersulfone (PES) substrates to prepared a novel nanofiltration membranes [16] and PEI functionalized nanofibrous membrane utilizing PDA as a mediator for Cu^{2+} removal [17]. The PDA and PEI functionalized magnetic composites have both the magnetic separation properties of Fe_3O_4 and the excellent adsorption properties of PEI to contaminants. PEI@PDA@Fe_3O_4 was prepared with PEI and PDA, PEI was covalently grafted onto the Fe_3O_4 surface by a Michael addition reaction and/or a Schiff base reaction with the quinone functional group of PDA layer [16].

In the present study, PEI@PDA@Fe_3O_4 was prepared and characterized and its property of adsorption toward methyl orange dye (MO, molecular weight 327.33 g/mol, common acidic/anionic dye) from solution was presented. The adsorption of MO from aqueous solution was carried out in batch mode and the process was evaluated through the kinetic, equilibrium and thermodynamic analyses.

2. Materials and methods

2.1. Materials

$FeCl_3{\cdot}6H_2O$ was purchased from Tianjin Fengchuan Chemical Reagent Technologies Co., Ltd. $FeSO_4{\cdot}7H_2O$ was supplied by Sinopharm Chemical Reagent Co., Ltd. Dopamine hydrochloride and ethylene imine polymer (molecular weight 10000 g/mol) were obtained from Aladdin Industrial Corporation of China. Methyl orange (MO) was purchased Tianjin Kemiou Chemical Reagent Co. , Ltd. All of the chemical agents were of analytical grade.

Stock solution of MO was prepared by dissolving MO in distilled water, and further diluted to the all working solution. Solution pH of MO was adjusted to the required value by an appropriate volume of 0.1 mol/L HCl and 0.1 mol/L NaOH. The concentration of MO was measured using a spectrophotometer at a wavelength corresponding to the maximum absorbance at 464 nm (752, Shanghai Shun Yu Hengping Science Instrument Co., Ltd, China).

2.2. Preparation of PEI@PDA@Fe_3O_4 particles

Fe_3O_4 was obtained by the co-precipitation method of ferric and ferrous ions in an acid solution. $FeCl_3{\cdot}6H_2O$ (5.41 g) and $FeSO_4{\cdot}7H_2O$ (5.57 g) were dissolved in 200 mL of 0.5 mol/L HCl solution. During the magnetic stirring at room temperature, 300 ml of 1.25 mol/L sodium hydroxide solution was added dropwise to the mixed solution. The final pH was adjusted to neutral with 25% HCl. The obtained precipitates, Fe_3O_4, were washed with distilled water several times, and then collected and heated at 333 K and stored in a glass bottle.

Fe_3O_4 modified with polydopamine (PDA@Fe_3O_4) was prepared by a certain amount of Fe_3O_4 with 1.2 g/L dopamine solution. The dopamine solution was prepared by dissolving dopamine hydrochloride in 0.01 mol/L Tris-HCl buffer at pH 8.5. The mechanical stirring time for the coated process was 4 h with ice bath and 2 h at room temperature. Then the solid was separated by external magnet and was washed with distilled water several times until pH of the solution was the same as that of the distilled water. Therefore, the PDA@Fe_3O_4 was obtained and dried at 333K and stored for further use.

The PDA@Fe_3O_4 was immersed into the 2 g/L PEI aqueous solutions at 333K with magnetic stirring for 4 h [18]. Fig. 1 was the schematic diagram of preparation. Then the magnetic core-shell polyethylenimine/polydopamine/Fe_3O_4 (PEI@PDA@Fe_3O_4) composites were rinsed thoroughly with distilled water. Finally, PEI@PDA@Fe_3O_4 was dried at 333K and collected in an airtight glass bottle.

2.3. Characterization of Fe_3O_4 and PEI@PDA@Fe_3O_4

The common elements were used by Automatic Element Analyzer (EA, Thermo Flash EA 1112, American). The X-Ray Diffractometer (XRD, PANalytical X´Pert PRO, Holland) was applied to identify the mineral phases. The microstructure and morphology of Fe_3O_4 and PEI@PDA@Fe_3O_4 particles were imaged by scanning electron microscopy (SEM, Hitachi Su8020, Japan). The pH at point zero charge (pH_{pzc}) of Fe_3O_4@La-Ce was evaluated by the 0.01 mol/L NaCl solid addition method.

2.4. Adsorption experiments

The removal of MO from aqueous solution by PEI@PDA@Fe_3O_4 was studied in batch mode. A certain amount of absorbent was placed in a 50 mL erlenmeyer flask, into which added 10 mL of MO solution of initial concentration of 50 mg/L. The batch adsorption was carried out in air bath (Guohua enterprise SHZ-82, China) at 120 rpm. The effect factors included: (1) compare the adsorption capacities of MO on Fe_3O_4 (0.50 g/L), PDA@Fe_3O_4 (0.50 g/L) and PEI@PDA@Fe_3O_4 (0.50 g/L): contact time was 10 h at a constant temperature 303K, pH unadjusted; (2) effect of adsorbent dose: (0.10~3.60 g/L) at the temperature of 303 K for 12 h, pH unadjusted; (3) effect of pH: (2–12) at a constant temperature 303 K, PEI@PDA@Fe_3O_4 (0.50 g/L); (4) effect of co-existing anions: different concentrations of NaCl, Na_2SO_4 solution (0.02, 0.04, 0.06 and 0.08 mol/L, respectively) at a constant temperature 303 K, pH 3, PEI@PDA@Fe_3O_4 (0.50 g/L); (5) effect of contact time: (5~300 min) at constant temperature 303 K and different concentrations (50 mg/L, 80 mg/L and 130 mg/L), pH 3, PEI@PDA@Fe_3O_4 (0.50 g/L); (6) effect of adsorption temperature: (293 K, 303 K and 313 K) at different concentrations range from 10 to 150 mg/L, pH 3, PEI@PDA@Fe_3O_4 (0.50 g/L).

The adsorption capacity (q_t or q_e, mg/g) of MO onto unit weight of PEI@PDA@Fe_3O_4 and removal percentage was calculated according to the following equations:

$$q = \frac{V(C_0 - C)}{m} \tag{1}$$

$$p = \frac{C_0 - C}{C_0} \tag{2}$$

where C_0 is the initial MO concentration (mg/L), C is the MO concentration at any time t or equilibrium (mg/L), V is the MO solution volume (L), and m is the mass of the adsorbent (g).

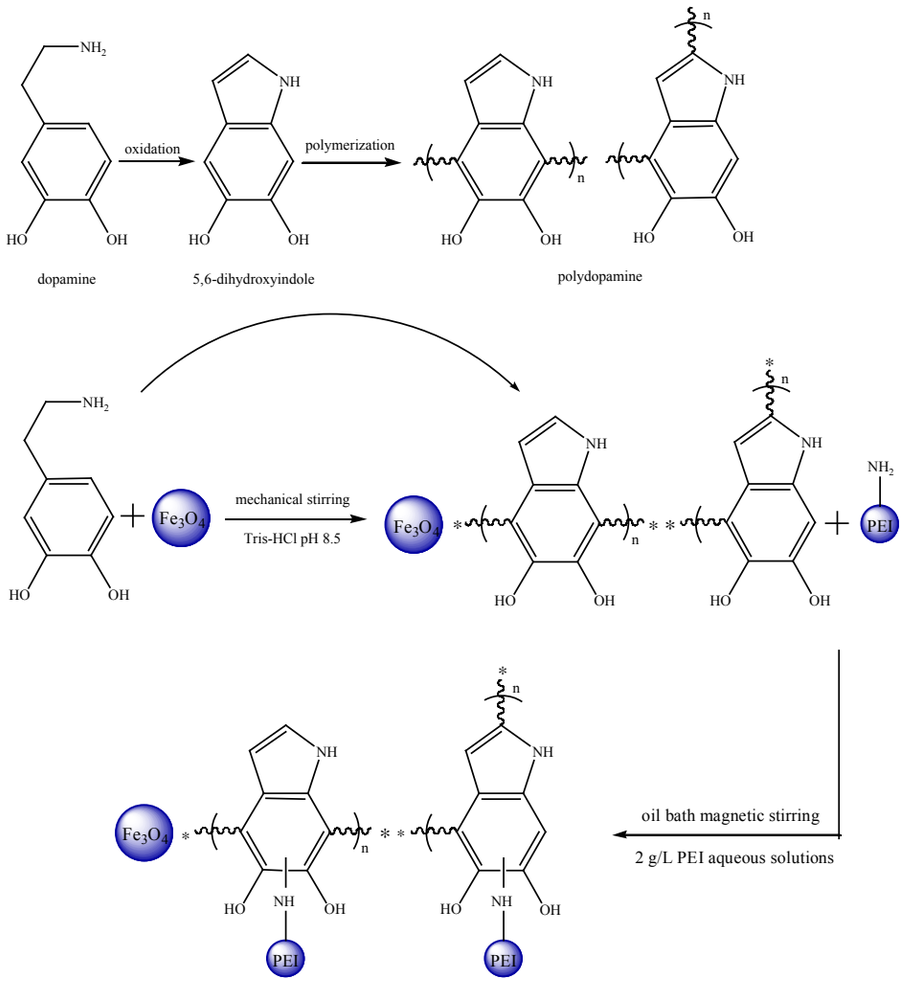

Fig. 1. Schematic diagram of the process with PDA and PEI of Fe_3O_4 surface functionalization.

2.5. Desorption study

The exhausted or MO-loaded PEI@PDA@Fe_3O_4 was obtained for the adsorption of 130 mg/L of MO at pH 3.0. Then, MO-loaded PEI@PDA@Fe_3O_4 was washed with distilled water to remove any unabsorbed dye and was dried at 333 K. The exhausted adsorbent was regenerated by 0.01 mol/L HCl solution. The regenerated PEI@PDA@Fe_3O_4 was reused at the same experimental conditions. The regeneration yield was obtained as the ratio of values of q_e before and after regeneration.

3. Results and discussion

3.1. Characterization of materials

The percentages of common elements were obtained by elemental analysis. The percentages of common elements were 0.14% N, 0.08% C, 0.32% H for Fe_3O_4 and 2.38% N, 8.18% C, 1.17% H for PEI@PDA@Fe_3O_4, respectively. The increased percentages of N, C and H about PEI@PDA@Fe_3O_4 were from the surface of PEI and PDA. The XRD patterns of the Fe_3O_4 and PEI@PDA@Fe_3O_4 are shown in Fig. 2. The Fe_3O_4 and PEI@PDA@Fe_3O_4 displayed similar characteristic peaks at 35.4°, 56.9°, 62.5° assigned to magnetite FeO·Fe_2O_3. The coating by PEI and PDA did not bring about the emergence of any new peaks, which indicated that PEI, PDA on the surface of magnetite might not change the crystal structures of Fe_3O_4. Moreover, PEI and PDA on the surface of magnetite could all be regarded as amorphous phase without a certain crystal structure. SEM photographs in Fig. 3 were taken at 50000×, 10000× magnifications to observe the surface of Fe_3O_4 and PEI@PDA@Fe_3O_4, respectively. It was seen that the Fe_3O_4 and PEI@PDA@Fe_3O_4 particles appeared as grains with sizes ranging from 100 nm to 5 um. The coated Fe_3O_4 surfaces were apparently the formation of PEI and PDA during the modified process, and the PEI@PDA@Fe_3O_4 particles were more dispersible and rougher after the improved process.

Fig. 4 was to measure the point zero charge of Fe_3O_4 and PEI@PDA@Fe_3O_4 in solution. The pH_{pzc} values from Fig. 4 indicated that the chemical pretreatment of Fe_3O_4 caused an increase of pH_{pzc}, changing the acidic surface of Fe_3O_4 (pH_{pzc} 5.6) to basic one for PEI@PDA@Fe_3O_4 (pH_{pzc} 7.7). The

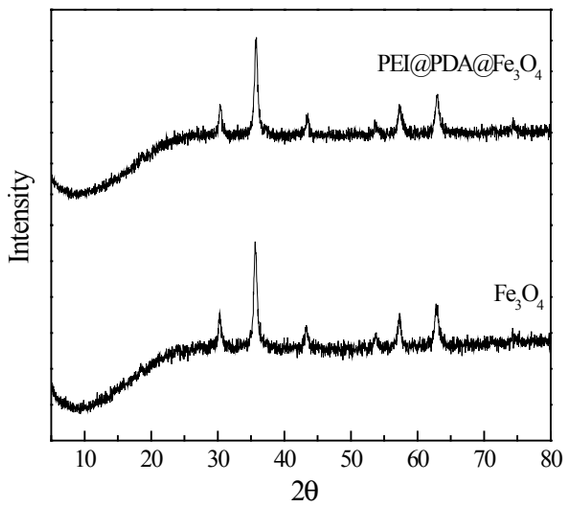

Fig. 2. XRD spectra of Fe_3O_4 and PEI@PDA@Fe_3O_4.

improvement of pH_{pzc} suggested coated PDA and immobilization of PEI.

The analysis of FTIR (figure not shown) was also performed. Peaks located at 3405 cm^{-1} and 1622 cm^{-1} from Fe_3O_4 were due to vibration of –OH from absorbed water and strong peak at 580 cm^{-1} was from vibration of Fe–O. Peaks at 3426, 1625, 1285 cm^{-1} (relative to vibration of –OH, $–NH_2$ and C–O from PDA) became stronger after PDA modification. The broad overlapping peak at 3416 cm^{-1} became stronger as a large number of amine groups from PEI were introduced on the surface. The peak evident at 1127 cm^{-1} was due to the C–N stretching vibration. So it can be concluded that PEI be successfully coated on surface of Fe_3O_4.

3.2. Adsorption study

3.2.1. Comparative studies of adsorption capacities of MO on various materials

Comparison of adsorption quantity among Fe_3O_4, PDA@Fe_3O_4 and PEI@PDA@Fe_3O_4 is presented in Fig. 5

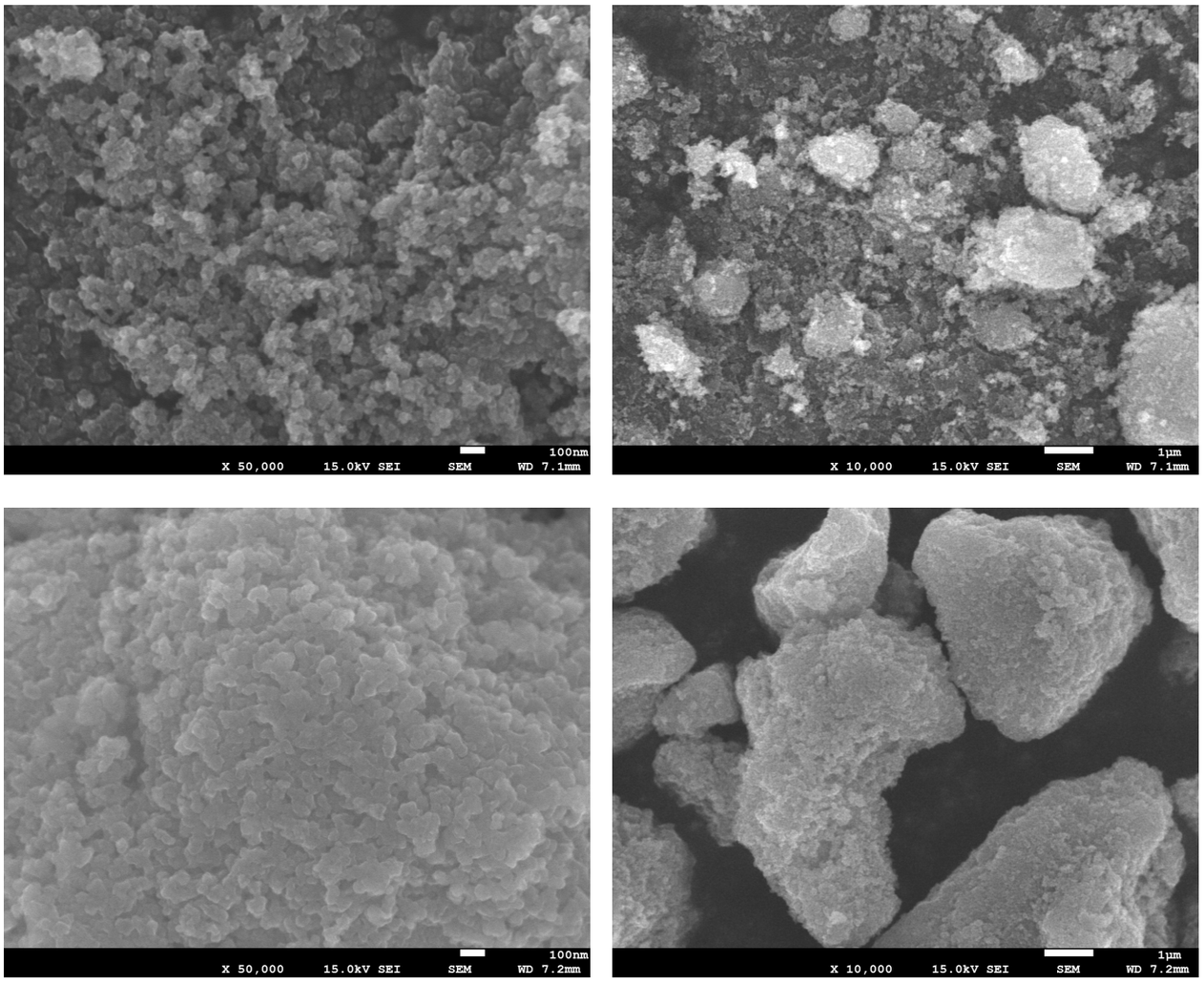

Fig. 3. SEM micrograph of Fe_3O_4 (a, b) and PEI@PDA@Fe_3O_4 (c, d).

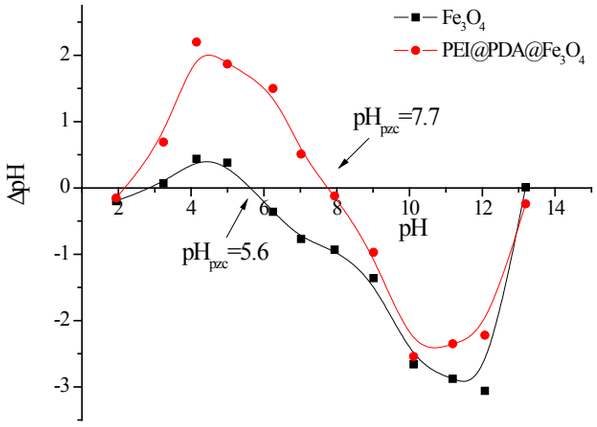

Fig. 4. The point zero charge of Fe_3O_4 and PEI@PDA@Fe_3O_4.

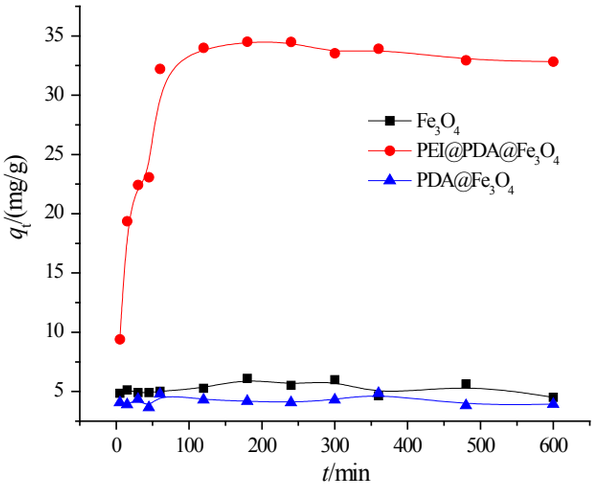

Fig. 5. Comparison of the adsorption capacity of MO onto Fe_3O_4, PDA@Fe_3O_4 and PEI@PDA@Fe_3O_4.

at various contact time. It was shown that the adsorption quantities were 4.30, 3.94, 34.2 mg/g for Fe_3O_4, PDA@Fe_3O_4 and PEI@PDA@Fe_3O_4, respectively. The PEI@PDA@Fe_3O_4 with higher adsorption ability was attributed to PEI-based adsorbents with good adsorption capacity toward anionic ions, such as negatively charged organic or inorganic substances, including various anionic dyes [19]. It was also observed that adsorption capacity increased significantly in the initial stage, and then increased at a slow rate, until reaching the adsorption equilibrium after 120 min. In the initial stage, most of the vacant surface sites were available for adsorption. Then the adsorption of MO was gradual adsorption stage and finally the MO uptake reached equilibrium.

3.2.2 *Effect of adsorbent dose on adsorption*

Adsorbent dose is also effective to remove adsorbates from solution. The effect of adsorbent dose on adsorption is shown in Fig. 6. The results showed that the removal

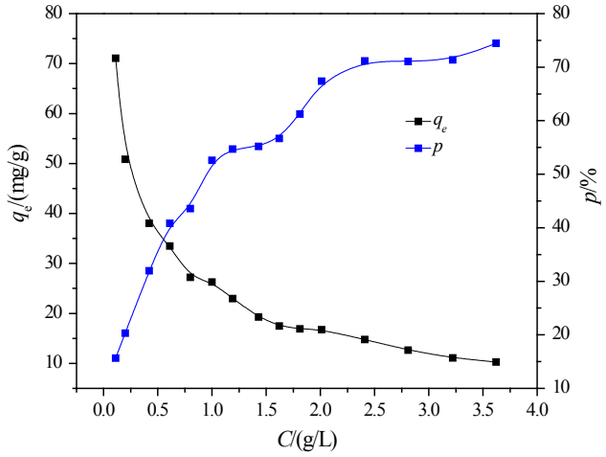

Fig. 6. Effect of adsorbent dose on MO adsorption.

percentage of MO increased from 15.6 % to 74.4 % and the values of q_e decreased from 71.1 mg/g to 10.3 mg/g when the adsorbent dose increased from 0.1 to 3.6 g/L. The main reason was that the number of sites available for adsorption sites also increased with the increase of adsorption dose. However, even though the removal efficiency of MO increased, the adsorption quantity decreased with the increase of adsorbent dosage. The reduction in adsorption quantity may be due to the overlap or aggregation of the adsorption sites resulting in a decrease in the adsorption surface area and an increase in the length of the diffusion path [20]. In the experimental application, considering the increase of adsorption efficiency and adsorption quantity, 0.5 mg/L of adsorbent dose was chosen in other study.

3.2.3. *Effect of pH on adsorption*

Solution pH often plays important role in adsorption process as pH can affect the existed form of adsorbate and surface property of adsorbent. Fig. 7 shows the effect of initial solution pH on MO adsorption quantity by PEI@PDA@Fe_3O_4. The amount of adsorption increased first and then decreased with the increase of pH, and the maximum adsorption capacity of MO occurred at pH 3 MO was anthraquinone or azo bond depends on the pH. When the pH was less than 3, the tertiary amine in the MO molecule was positively charged due to protonation and the electrostatic effect was weakened to reduce the adsorption capacity. The removal of dye adsorbed decreased sharply of pH 3~8, while in the range of pH 8~12, the adsorption capacity decreased slowly with the increase of pH. The surface charge assessed by point of zero charge of PEI@PDA@Fe_3O_4 was about 7.7. When the solution pH was below 7.7, the surface of PEI@PDA@Fe_3O_4 was positive charge due to the protonation of the amino groups, enhancing the electrostatic attraction between the anionic MO and the adsorption sites of the PEI@PDA@Fe_3O_4. However, when the solution pH value was 8, the adsorption capacity could still reach 22.2 mg/g, which might be attributed to the ion exchange and other action between the adsorbent and adsorbate. When the pH of the solution was greater than 7.7, the sur-

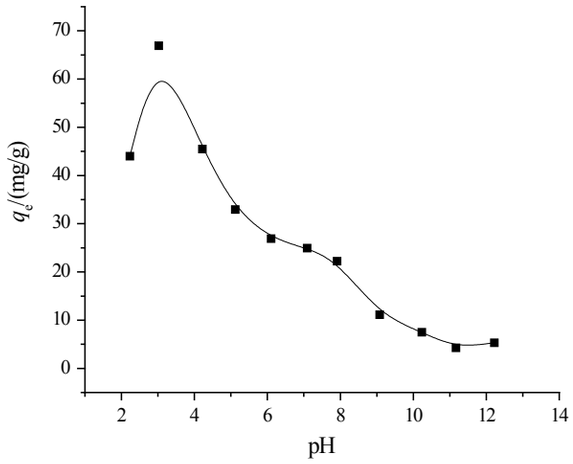

Fig. 7. Effect of solution pH on MO adsorption.

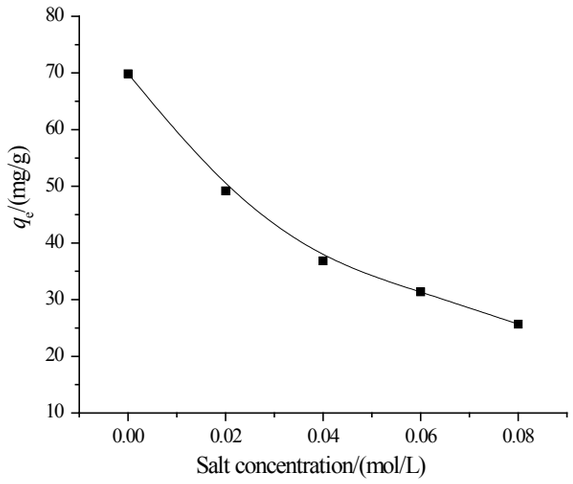

Fig. 8. Effect of common salts on MO adsorption.

face charge of the deprotonated adsorbent became negative, and the electrostatic repulsion was not favor of adsorption of anionic dyes which caused an evident decrease in the MO adsorption. At the same time, a large amount of OH^- in the solution may compete with MO anionic dyes, also resulting in the decrease of adsorption on PEI@PDA@Fe_3O_4 adsorption decreased.

The similar results about effect of pH were also observed in study of MO adsorption onto chitosan coated on quartz sand [21] and MO adsorption onto cationic surfactant-modified wheat straw [22].

3.2.4. Effect of common salts on adsorption

It is necessary to study the effect of coexisted salt in solution on adsorption quantity as there are common salts in dye wastewater. The results are shown in Fig. 8. It was shown that values of q_e decreased from 69.8 to 25.6 mg/g as the concentration of NaCl was to 0.08 mol/L. There may be competitive adsorption between Cl^- ions and anionic MO for binding sites, which negatively affected the electrostatic attraction between PEI@PDA@Fe_3O_4 and MO. Furthermore, as the ionic strength (NaCl concentration) increased, the activity of MO and the active sites decreased, thereby reduced the adsorption quantity. It can be referred that electrostatic attraction may be main mechanism according to the results obtained from effect of solution pH and salt concentration.

Similar result was observed about MO adsorption onto chitosan coated on quartz sand [21]. But in other system, there was in favor of adsorption when salt concentration increased, such as MO adsorption onto cationic surfactant-modified wheat straw [22] and congo red adsorption onto PEI modified wheat straw [23]. The various results may be the difference of main mechanism.

3.2.5. Adsorption kinetic study

Fig. 9 shows the effect of contact time on adsorption quantity at three initial MO concentrations. It is shown in Fig. 9 that the adsorption kinetic curves were initially rapidly in 60 min, then raised slowly from 60 to 120 min, and kept equilibrium after 120 min.

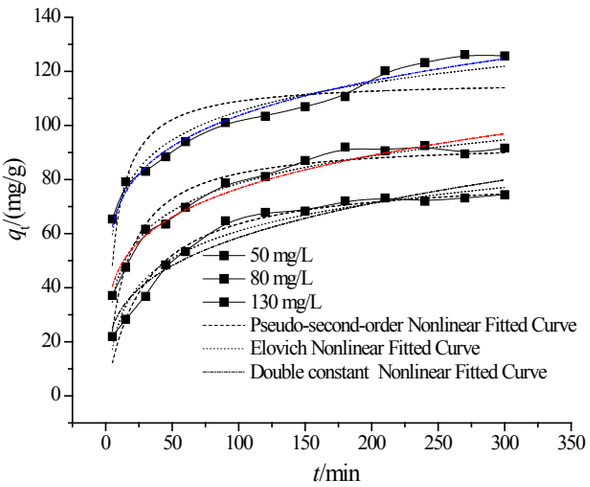

Fig. 9. Effect of contact time on MO adsorption.

In order to investigate the time dependent adsorption data further, the pseudo-second-order model, Elovich equation and Double Constant equation were used to describe the kinetics. The pseudo-second-order model is also applied to assess the chemical adsorption mechanism involving electron sharing or electron transfer of the MO absorbed concentration [10]. Elovich model is used to describe the process where the activation energy has a great change [24]. Double Constant model is an empirical equation and the experimental application shows that it is also applicable to the complicated kinetic process of the reaction process.

The expressions of three kinetic models were following:

Pseudo-second-order kinetic model:

$$q_t = \frac{k_2 q_e^2 t}{1 + k_2 q_e t} \tag{3}$$

Elovich equation:

$$q_t = \frac{\ln(\alpha\beta)}{\beta} + \frac{\ln t}{\beta} \quad (4)$$

Double constants equation:

$$q_t = At^{K_s} \quad (5)$$

where q_t is adsorption quantity (mg/g) at time t, q_e is adsorption quantity at equilibrium (mg/g); k_2 is pseudo-second-order kinetic rate constant (mg/g min); α is the initial adsorption rate constant (mg/g min) and the parameter β is related to the extent of surface coverage and activation energy for chemisorption (g/mg); A is constant, K_s is adsorption rate coefficient.

The kinetic data were treated by nonlinear regressive analysis and the fitted curves are also shown in Fig. 9. The parameters of kinetic models and determined coefficients (R^2) and errors (SSE) are summarized in Table 1. From Table 1, the adsorption of MO on PEI@PDA@Fe_3O_4 can be better described by both the Elovich equation and Double Constant equation with higher values of R^2 and lower values of SSE. It can be concluded that the adsorption system be an ion exchange process and heterogeneous diffusion process.

3.2.6. Adsorption isotherm

The effect of equilibrium MO concentration and solution temperature on adsorption quantity are performed and the results are presented in Fig. 10. It was observed that the value of q_e for MO adsorption increased with the increase of MO concentration, then reached a plateau. This could be attributed to the driving force from the dye concentration gradient. Moreover, adsorption quantity became larger with the increase of temperature, which indicted an endothermic process during MO adsorption. The larger values of $q_{e(exp)}$ obtained at 293, 303 and 313 K were 120, 129 and 133 mg/g, respectively, which showed that the effect of temperature on adsorption quantity was not significant and there is slight increase of adsorption quantity at higher temperature. But other researches found that there was not favor of MO adsorption with the increase of temperature such as MO adsorption onto chitosan coated on quartz sand [21] and cationic surfactant-modified wheat straw [22].

Table 1
Parameters of kinetic models for MO adsorption onto PEI@PDA@Fe_3O_4

C_0 (mg/L)	50	80	130
Pseudo-second-order kinetic equation			
$q_{e(exp)}$ (mg/g)	74.4	92.5	126
$q_{e(theo)}$ (mg/g)	81.8	94.3	117
k_2	4.28E-04	7.24E-04	1.21E-03
R^2	0.962	0.911	0.697
SSE	145	331	1.25E+03
Elovich equation			
α	9.48	31.2	154
β	6.84E-02	6.82E-02	6.58E-02
R^2	0.957	0.976	0.943
SSE	162	87.4	234
Double constants eqaution			
A	16.0	28.7	47.8
K_s	0.282	0.213	0.168
R^2	0.933	0.962	0.974
SSE	253	142	107

Note: SSE= $\sum(q-q_c)^2$, q and q_c are the experimental value and calculated value according the model, respectively

The isothermal models indicate the surface properties of adsorbents, the adsorption behavior and the adsorption system, giving a fully understand of the sorption capacity of adsorbed molecules. In this study, the equilibrium data were analyzed using Langmuir model, Freundlich model and Koble-Corrigan model.

The Langmuir model assumes that a monolayer is formed without interaction between adsorbed molecules when adsorption occurs. The equation of Langmuir isotherm is as follows [25]:

$$q_e = \frac{q_m K_L c_e}{1 + K_L c_e} \quad (6)$$

where q_m is the maximum adsorption capaticity (mg/g), q_e is the equilibrium adsorption capacity (mg/g), K_L is a constant related to the affinity of the binding sites and energy of adsorption (L/mg). C_e is equilibrium concentration (mg/L).

The Freundlich isotherm describes a non-ideal adsorption method for heterogeneous surface as well as for multilayer adsorption by assuming an exponentially decaying adsorption point energy distribution [26]. The Freundlich isotherm equation can be expressed by the following equation:

$$q_e = K_F c_e^{1/n} \quad (7)$$

where K_F is the constant of the Freundlich isotherm, $1/n$ is the constant which related to the adsorption capacity and the adsorption intensity.

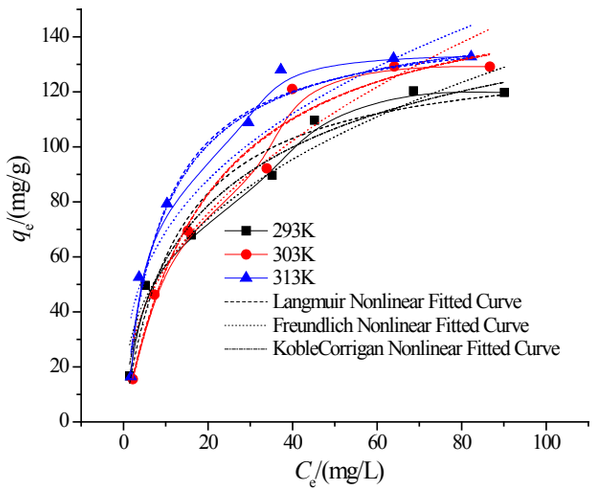

Fig. 10. Adsorption isotherms of MO at various temperatures.

The Koble-Corrigan isotherm is a three-parameter model, which is a combination of Langmuir and Freundlich isotherm models. When n = 1, Koble Corrigan isotherm is converted to Langmuir isotherm. When B = 0, the equation is converted to Freundlich isotherm [27]. The Koble-Corrigan isotherm can be represented as:

$$q_e = \frac{AC_e^n}{1 + BC_e^n} \tag{8}$$

where A, B and n are the Koble-Corrigan isotherm constants.

The isotherm model parameters were estimated by nonlinear regressive method and the results are listed in Table 2. The obtained values of $1/n$ between 0.1 and 0.5, confirmed a higher adsorption capacity of MO at all temperatures. Base on the values of R^2 and SSE, Langmuir model and Koble-Corrigan model were better to describe the adsorption in MO/ PEI@PDA@Fe_3O_4 system. The constant g was close to 1, indicating that the isotherm was close to the Langmuir isotherm.

From a practical point of view, the feasibility of Langmuir isotherm can be explained in term of the separation factor (R_L), a dimensionless factor. It can be expressed by the following equation [28]:

$$R_L = \frac{1}{1 + K_L C_0} \tag{9}$$

where C_0 is initial MO concentration and K_L is Langmuir constant. The value of R_L indicates the type of the isotherm: unfavorable adsorption ($R_L > 1$), favorable adsorption ($0 < R_L < 1$), linear adsorption ($R_L = 1$), irreversible adsorption ($R_L = 0$). The R_L of MO adsorption onto PEI@PDA@Fe_3O_4 is in the range of 0.0779–0.559, 0.117–0.665 and 0.0555–0.469 for 293 K, 303 K and 313 K, respectively. It can describe the adsorption of MO by PEI@PDA@Fe_3O_4 was favorable adsorption process.

Table 2
Parameters of adsorption isotherm models for MO adsorption onto PEI@PDA@Fe_3O_4

T K	293	303	313
Langmuir model			
K_L (L/g)	7.89E-02	5.05E-02	1.13E-01
$q_{e(exp)}$ (mg/g)	120	129	133
q_m (mg/g)	136	165	147
R^2	0.957	0.964	0.950
SSE	328	356	502
Freundlich model			
K_F	24.4	20.8	31.0
$1/n$	0.370	0.432	0.349
R^2	0.955	0.914	0.895
SSE	350	856	1.06E+03
Koble Corrigan model			
A	18.4	7.71	18.0
B	0.101	0.048	0.119
n	0.673	1.03	0.944
R^2	0.968	0.955	0.938
SSE	197	355	498

The adsorption capacity of MO from Langmuir model about PEI@PDA@Fe_3O_4 and other adsorbents is listed in Table 3. It was evident that the MO adsorption capacity of PEI@PDA@Fe_3O_4 was larger than that most of the traditional adsorbents. In addition, PEI@PDA@Fe_3O_4 particle was prepared in aqueous solution and easily separated from solution, which was effective and environmentally friendly.

3.2.7. Thermodynamic parameters of adsorption

Thermodynamic parameters including enthalpy change (ΔH^o), Gibbs free energy change (ΔG^o) and entropy change (ΔS^o) estimated the effect of temperature on the adsorption of MO on PEI@PDA@Fe_3O_4. They can be determined using the following equations [35]:

$$K_c = C_{ad,e} / C_e \tag{9}$$

$$\Delta G^0 = -RT \ln K_c \tag{10}$$

$$\Delta G^0 = \Delta H^0 - T\Delta S^0 \tag{11}$$

where K_c is the distribution coefficient for the adsorption, $C_{ad,e}$ is the concentration of MO on the adsorbent at equilibrium (mg/L), R (8.314 J/(mol·K)) the universal gas constant, T temperature (K).

All the thermodynamic parameters are shown in Table 4. The all negative values of ΔG^o indicated the spontaneous nature, confirming the affinity of PEI@PDA@Fe_3O_4 for MO. The positive value of ΔH^o was 14.8 kJ/mol less than 40 kJ/mol, which confirmed the MO sorption on PEI@PDA@Fe_3O_4 was an endothermic and physical adsorption process [36]. The positive entropy change ΔS indicated that as MO moved from the hydrous phase to the surface of the PEI@PDA@Fe_3O_4, the degree of disorder increased and the

Table 3
Langmuir parameters of q_m toward MO about various adsorbents

Adsorbent	q_m (mg/g)	T K	Reference
PEI@PDA@Fe_3O_4	165	303	This study
Protonated cross-linked chitosan	131	303	[20]
Chitosan coated on quartz sand	49.0	293	[21]
Cationic surfactant-modified wheat straw	50.4	303	[22]
Acid modified carbon coated monolith	147	303	[28]
MgNiAl–CO_3	118	298	[29]
MgNiAl–C	375	298	[29]
γ-Fe_2O_3/SiO_2/chitosan composite	34.3	310	[30]
Polyaniline based on DBSNa	75.9	338	[31]
m-CS/γ-Fe_2O_3/MWCNTs	66.1	298	[32]
PAN-coated kapok hollow microtubes	34.7	298	[33]
Ammonium-functionalized silica nanoparticle	105.4	293	[34]

Table 4
Thermodynamic parameters of MO adsorption onto PEI@PDA@Fe_3O_4

ΔH^0 (kJ/mol)	ΔS^0 (J/(mol·K))	ΔG^0 (kJ/mol)		
		293K	303K	313K
14.8	63.5	−3.83	−5.10	−2.85

number of species on the solid / liquid interface increased [12]. In general, the thermodynamic parameters indicated that the adsorption was spontaneous and endothermic.

3.2.8. Desorption study

Desorption study helpful to explain the mechanism of adsorption process and to make the adsorption process more economical [37–40]. The regenerated efficiency of three cycles was 140%, 71.8% and 61.3%, respectively. It was over 100% because the adsorption was not saturated at first time. Regeneration efficiency gradually decreased after three cycles. There was some efficient to reuse MO-loaded adsorbent using 0.010 mol/L HCl solution. This also implied that the attachment of MO onto PEI@PDA@Fe_3O_4 be through ion exchange or electrostatic attraction.

4. Conclusions

PEI@PDA@Fe_3O_4 was prepared and the property of MO adsorption from aqueous solution was investigated in bath mode. PEI and PDA were successfully loaded onto the Fe_3O_4 surface through characterization. The best solution pH for adsorption was pH 3 and the existence of salts was disadvantage of MO adsorption. Kinetics data tend to fit well in Elovich equation and Double Constant model while the equilibrium data were best fitted by Langmuir and Koble Corrigan models. The MO adsorption processes was spontaneous and endothermic in nature. There is some property of reuse after regeneration of MO-loaded adsorbent.

Acknowledgements

This work was supported by the National Natural Science Foundation of China for undergraduate cultivation in basic science (J0830412).

References

[1] A. Bafana, S.S. Devi, T. Chakrabarti, Azo dyes: past, present and the future, Environ. Rev., 19 (2011) 350–370.
[2] Y. Fan, H.J. Liu, Y. Zhang, Y. Chen, Adsorption of anionic MO or cationic MB from MO/MB mixture using polyacrylonitrile fiber hydrothermally treated with hyperbranched polyethylenimine, J. Hazard. Mater., 283 (2015) 321–328.
[3] R.D.G. Franca, A. Vieira, A.M.T. Mata, G.S. Carvalho, H.M. Pinheiro, N.D. Lourenco, Effect of an azo dye on the performance of an aerobic granular sludge sequencing batch reactor treating a simulated textile wastewater, Water Res., 85 (2015) 327–336.
[4] S.K. Nataraj, K.M. Hosamani, T.M. Aminabhavi, Nanofiltration and reverse osmosis thin film composite membrane module for the removal of dye and salts from the simulated mixtures, Desalination, 249 (2009) 12–17.
[5] A.K. Verma, R.R. Dash, P. Bhunia, A review on chemical coagulation/flocculation technologies for removal of colour from textile wastewaters, J. Environ. Manage., 93 (2012) 154–168.
[6] T. Chen, C. Yan, Y. Wang, C. Tang, S. Zhou, Y. Zhao, R. Ma, P. Duan, Synthesis of activated carbon-based amino phosphonic acid chelating resin and its adsorption properties for Ce(III) removal, Environ. Technol., 36 (2015) 2168–2176.
[7] T. Zhou, W.Z. Lu, L.F. Liu, H.M. Zhu, Y.B. Jiao, S.S. Zhang, R.P. Han, Effective adsorption of light green anionic dye from solution by CPB modified peanut in column mode, J. Mol. Liqd., 211 (2015) 909–914.
[8] Y.Y. Su, B.L. Zhao, W. Xiao, R.P. Han, Adsorption behavior of light green anionic dye using cationic surfactant-modified wheat straw in batch and column mode, Environ. Sci. Pollut. Res., 20 (2013) 5558–5568.
[9] V. Rocher, J.-M. Siaugue, V. Cabuil, A. Bee, Removal of organic dyes by magnetic alginate beads, Water Res., 42 (2008) 1290–1298.
[10] H. Zhang, Q. Luan, H. Tang, F.H. Huang, M.M. Zheng, Q.C. Deng, X. Xiang, C. Yang, J. Shi, C. Zheng, Q. Zhou, Removal of methyl orange from aqueous solutions by adsorption on cellulose hydrogel assisted with Fe_2O_3 nanoparticles, Cellulose, 24 (2016) 903–914.
[11] L. Lai, Q. Xie, L.N. Chi, W. Gu, D.Y. Wu, Adsorption of phosphate from water by easily separable Fe_3O_4@SiO_2 core/shell magnetic nanoparticles functionalized with hydrous lanthanum oxide, J. Colloid Interface Sci., 465 (2016) 76–82.
[12] L.G. Yan, K. Yang, R.R. Shan, T. Yan, J. Wei, S.J. Yu, H.Q. Yu, B. Du, Kinetic, isotherm and thermodynamic investigations of phosphate adsorption onto core-shell Fe_3O_4@LDHs composites with easy magnetic separation assistance, J. Colloid Interface Sci., 448 (2015) 508–516.
[13] S.X. Dong, Y.L. Wang, Characterization and adsorption properties of a lanthanum-loaded magnetic cationic hydrogel composite for fluoride removal, Water Res., 88 (2016) 852–860.
[14] Y. Liu, X.S. Zhao, X.J. Pan, B. Chen, Removal of methyl orange by polyethylenimine/Fe_3O_4 hybrid magnetic nanoadsorbents, Chin. J. Environ. Eng., 10 (2016) 1152–1158. (in Chinese)
[15] H. Lee, S.M. Dellatore, W.M. Miller, P.B. Messersmith, Mussel-inspired surface chemistry for multifunctional coatings, Science, 318 (2007) 426–430.
[16] R.N. Zhang, Y.L. Su, X.T. Zhao, Y.F. Li, J.J. Zhao, Z.Y. Jiang, A novel positively charged composite nanofiltration membrane prepared by bio-inspired adhesion of polydopamine and surface grafting of poly(ethylene imine), J. Membr. Sci., 470 (2014) 9–17.
[17] C.L. Wu, H.Y. Wang, Z. Wei, C. Li, Z.D. Luo, Polydopamine-mediated surface functionalization of electrospun nanofibrous membranes: Preparation, characterization and their adsorption properties towards heavy metal ions, Appl. Surf. Sci., 346 (2015) 207–215.
[18] L.F. Bai, S.X. Duan, W.Q. Jiang, M. Liu, S. Wang, M. Sang, X.L. Gong, J.X. Li, S.H. Xuan, High performance polydopamine-functionalized mesoporous silica nanospheres for U(VI) removal, Appl. Surf. Sci., 426 (2017) 1121–1132.
[19] Y. Ma, B.W. Zhang, H.J. Ma, M. Yu, L.F. Li, J.Y. Li, Polyethylenimine nanofibrous adsorbent for highly effective removal of anionic dyes from aqueous solution, Sci. China Mater., 59 (2016) 38–50.
[20] R.H. Huang, Q. Liu, J. Huo, B.C. Yang, Adsorption of methyl orange onto protonated cross-linked chitosan, Arab. J. Chem., 10 (2017) 24–32.
[21] B.L. Zhao, X.N. Zhang, C.C. Dou, R.P. Han, Adsorption property of methyl orange by chitosan coated on quartz sand in batch mode, Desal. Water Treat., 55 (2015) 1598–1608.
[22] Y.Y. Su, Y.B. Jiao, CC. Dou, R.P. Han, Biosorption of methyl orange from aqueous solutions using cationic surfactant-modified wheat straw in batch mode, Desalin. Water Treat., 52 (2014) 6145–6155.
[23] Y. Shang, J.H. Zhang, X. Wang, R.D. Zhang, W. Xiao, S.S. Zhang, R.P. Han, Use of polyethylenemine modified wheat straw for adsorption of congo red from solution in batch mode, Desal. Water Treat., 57 (2016) 8872–8883.

[24] R.D. Zhang, J.H. Zhang, X.N. Zhang, C.C. Dou, R.P. Han, Adsorption of Congo red from aqueous solutions using cationic surfactant modified wheat straw in batch mode: Kinetic and equilibrium study, J. Taiwan Inst. Chem. E., 45 (2014) 2578–2583.
[25] J.J. Chen, X.W. Shi, Y.F. Zhan, X.D. Qiu, Y.M. Du, H.B. Deng, Construction of horizontal stratum landform-like composite foams and their methyl orange adsorption capacity, Appl. Surf. Sci., 397 (2017) 133–143.
[26] N. Farnad, K. Farhadi, N.H. Voelcker, Polydopamine nanoparticles as a new and highly selective biosorbent for the removal of copper (II) ions from aqueous solutions, Water Air Soil Poll., 223 (2012) 3535–3544.
[27] H.M. Zhu, M.M. Zhang, Y.Q. Liu, L.J. Zhang, R.P. Han, Study of congo red adsorption onto chitosan coated magnetic iron oxide in batch mode, Desal. Water Treat., 37 (2012) 46–54.
[28] W. Cheah, S. Hosseini, M.A. Khan, T.G. Chuah, T.S.Y. Choong, Acid modified carbon coated monolith for methyl orange adsorption, Chem. Eng. J., 215 (2013) 747–754.
[29] H. Zaghouane-Boudiaf, M. Boutahala, L. Arab, Removal of methyl orange from aqueous solution by uncalcined and calcined MgNiAl layered double hydroxides (LDHs), Chem. Eng. J., 187 (2012) 142–149.
[30] H.Y. Zhu, R. Jiang, Y.Q. Fu, J.H. Jiang, L. Xiao, G.M. Zeng, Preparation, characterization and dye adsorption properties of gamma-Fe_2O_3/SiO_2/chitosan composite, Appl. Surf. Sci., 258 (2011) 1337–1344.
[31] M. Tanzifi, S.H. Hosseini, A.D. Kiadehi, M. Olazar, K. Karimipour, R. Rezaiemehr, I. Ali, Artificial neural network optimization for methyl orange adsorption onto polyaniline nano-adsorbent: Kinetic, isotherm and thermodynamic studies, J. Mol. Liq., 244 (2017) 189–200.
[32] H.Y. Zhu, R. Jiang, L. Xiao, G.M. Zeng, Preparation, characterization, adsorption kinetics and thermodynamics of novel magnetic chitosan enwrapping nanosized gamma-Fe_2O_3 and multi-walled carbon nanotubes with enhanced adsorption properties for methyl orange, Bioresour. Technol., 101 (2010) 5063–5069.
[33] A.R. Agcaoili, M.U. Herrera, C.M. Futalan, M.D.L. Balela, Fabrication of polyacrylonitrile-coated kapok hollow microtubes for adsorption of methyl orange and Cu(II) ions in aqueous solution, J. Taiwan Inst. Chem. E., 78 (2017) 359–369.
[34] J.S. Liu, S. Ma, L.J. Zang, Preparation and characterization of ammonium-functionalized silica nanoparticle as a new adsorbent to remove methyl orange from aqueous solution, Appl. Surf. Sci., 265 (2013) 393–398.
[35] Y.L. Liu, X.R. Zhao, J.L. Li, D. Ma, R.P. Han, Characterization of bio-char from pyrolysis of wheat straw and its evaluation on methylene blue adsorption, Desal. Water Treat., 46 (2012) 115–123.
[36] J.W. Fu, Z.H. Chen, M.H. Wang, S.J. Liu, J.H. Zhang, J.N. Zhang, R.P. Han, Q. Xu, Adsorption of methylene blue by a high-efficiency adsorbent (polydopamine microspheres): Kinetics, isotherm, thermodynamics and mechanism analysis, Chem. Eng. J., 259 (2015) 53–61.
[37] Z.W. Wang, P. Han, Y.B. Jiao, X.T. He, C.C. Dou, R.P. Han, Adsorption of Congo red using ethylenediamine modified wheat straw, Desal. Water Treat., 30 (2011) 195–206.
[38] R.P. Han, Y. Wang, Q. Sun, L.L. Wang, J.Y. Song, X.T. He, C.C. Dou, Malachite green adsorption onto natural zeolite and reuse by microwave irradiation, J. Hazard. Mater., 175 (2010) 1056–1061.
[39] Y.B. Jiao, D.L. Han, Y.Z. Lu, Y.C. Rong, L.Y. Fang, Y.L. Liu, R.P. Han, Characterization of pine-sawdust pyrolytic char activated by phosphoric acid through microwave irradiation and adsorption property toward CDNB in batch mode, Desal. Water. Treat., 77 (2017) 247–255.
[40] J.S. Liu, G.N. Liu, W.X. Liu, Preparation of water-soluble β-cyclodextrin/poly(acrylic acid)/graphene oxide nanocomposites as new adsorbents to remove cationic dyes from aqueous solutions, Chem. Eng. J., 257 (2014) 299–308.